Universal short-time motion of a polymer in a random environment: Analytical calculations, a blob picture, and Monte Carlo results

Ute Ebert
Instituut-Lorentz, Universiteit Leiden, Postbus 9506, 2300 RA Leiden, The Netherlands

Artur Baumgärtner
Institut für Festkörperforschung, Forschungszentrum Jülich G.m.b.H., 52425 Jülich, Germany

Lothar Schäfer
Fachbereich Physik, Universität Essen, 45117 Essen, Germany
(Received 29 August 1995)

Using a recently established renormalization group approach [U. Ebert, J. Stat. Phys. (to be published)], we analyze the center-of-mass motion of a polymer in a Gaussian disordered potential. While in the long-time limit normal diffusion is found, we concentrate here on shorter times. We discuss the general structure of the relevant crossover scaling function and evaluate it quantitatively in three dimensions to one-loop order. We identify a universal short-time regime, where the chain length dependence of the center-of-mass motion is Rouse-like, while the time dependence is nontrivial. Motion in this regime can be interpreted in terms of a blob picture: A "time blob" defines an additional intrinsic length scale of the problem. The short-time dependence of the center-of-mass motion over several decades approximates a power law with an effective exponent that continuously depends on disorder (and also weakly on the time interval). We furthermore present the results of a simulation measuring the motion of a (pearl necklace) chain in Gaussian disorder in three dimensions. We find full agreement between theory and numerical experiment. The characteristic behavior found in these simulations closely resembles the results of some previous simulations aimed at seeing reptation. This suggests that such work was strongly influenced by energetic disorder or entropic traps.

PACS number(s): 36.20.Ey, 05.40.+j, 64.60.Ht

I. INTRODUCTION

Consider a very long polymer chain diffusing through a swollen gel or a diffraction column. The spatial distribution of matter in such a system is fairly random, but essentially does not change with time, even though the meshes of the gel fluctuate a little. We thus deal with the properties of a polymer embedded in some fixed but random environment ("quenched disorder"). The distribution of the random medium may be taken to be homogeneous in space, but in general will show strong spatial correlations. We concentrate here on an idealized model, where the range of these correlations is comparable to the size of the segments of our chain, while the size of the polymer coil for long chains is much larger. We thus will consider the segment size and the correlation length of the random medium as microscopic scales, small compared to the chain size. This allows us to derive universal results in a renormalizable theory.

Investigating a dynamic problem, besides the polymer size measured, e.g., as the radius of gyration R_G, there is a second obvious large length scale, namely, the root mean square diffusion length $R(t)$. It gives the average distance the center of mass of a polymer moves within time t. The relation $R_G = R(T_0)$ defines a time scale T_0, which discriminates the short-time from the long-time behavior. For short times $t < T_0$ we expect an anomaly of the time dependence due to disorder mediated autocorrelation effects of the polymer with its previous configuration. For long times $t \gg T_0$, the polymer essentially can be considered as an extended Brownian particle, which explores new parts of space with uncorrelated potentials. For space dimension $d > 0$ it then obeys a normal diffusion law $R^2(t) \propto t$ with a disorder reduced diffusion constant. (Note the difference of the lower critical dimension in this problem to random force models with a lower critical dimension of 2.) Explicit results for the renormalized diffusion constant in our special model to be defined below are derived in [1,2].

Besides the asymptotic diffusion constant, the short-time regime $t \lesssim T_0$ is also of interest because it yields additional information on the diffusion mechanism and it is more easily accessible to both computer or real experiments than the region $t \gg T_0$. Two of us already have published preliminary results [1] on the center-of-mass motion $R(t)$ for $t \ll T_0$. In the present paper we reinvestigate this problem. We present detailed analytical and numerical evaluations of our analytical results as well as Monte Carlo simulations. In the interplay of analytics and simulations we found a less obvious third length scale, which appears only in the short-time regime and plays a decisive role there. We denote this time-dependent scale as the root mean square radius $\ell_B(t)$ of

a "time blob" to be defined below. It shows up in a careful reinvestigation of the analytic expressions and allows us to consistently evaluate analytics and simulations.

While it was the analytic structure that lead us to introduce the concept of time blobs, on hindsight they are the natural physical quantities to appear in the short-time regime. Let us consider models in general, for which the displacements of the individual segments are due to local thermal fluctuations, i.e., let us consider models without long-range interactions such as, e.g., the hydrodynamic one. The assumption of hydrodynamic screening seems to be well justified in a random medium, as we conclude in analogy to the case of semidilute solutions [3]. Also, as mentioned above, we assume that the disorder does not introduce long-range correlations, which thus only are mediated by the extended structure of the chain itself. Consider now not the center-of-mass motion $R(t)$, but the dynamics of the single segments as appearing in the mean square distance of segments number i and j at times t' and $t+t'$

$$\mathcal{D}_{ij}(t) = \overline{\langle[\mathbf{r}_i(t+t') - \mathbf{r}_j(t')]^2\rangle}. \tag{1.1}$$

(The angular brackets denote the thermal average and the overbar the ensemble average.) Since the center-of-mass motion $R(t)$ results from summing over the individual displacements of the segments, it is rather $\mathcal{D}_{ij}(t)$ that traces the basic dynamics. For $t = 0$, $\mathcal{D}_{ij}(t)$ is determined by the static expectation value of the segment distance, while for $t \gg T_0$, $\mathcal{D}_{ij}(t)$ obviously can be approximated by $R^2(t)$, independent of i, j. For any given finite time t, there is a segment distance $|i-j|$ or a corresponding root mean square distance $\ell_B(t)$ in embedding space, at which the correlations cross over from being statically to being dynamically dominated. That means that for times $t' < t$, the behavior on the length scale $\ell_B(t)$ is dominated by the static correlations and segments, which are $\ell_B(t)$ apart from each other, undergo independent thermal fluctuations. For $t' > t$ in contrast, the segment correlations on the length scale $\ell_B(t)$ are dominated by joint diffusion. $\ell_B(t)$ thus defines the average size of the subchains that undergo correlated motion within the time t. For $\ell_B(t)$ we use the term "time blob" in analogy to the blob concept in semidilute static polymer solutions, since in both cases the interactions (in the one case due to the correlations induced by the quenched random medium and in the other case due to the excluded volume interaction) dominate the physics up to the blob size. With t growing, $\ell_B(t)$ grows continuously until it saturates at the size of the whole chain. $\ell_B(t_0) = R_G$ therefore defines another crossover time, viz., the time at which the displacements of the first and the last segment of the chain become correlated. T_0, in contrast, is the time the chain needs to diffuse a distance of the order of its own size. Obviously these two time scales are of the same order of magnitude and specifically they have the same dependence on chain length N in the whole class of models in which diffusion is driven by the uncorrelated local thermal displacements of the segments. We then can drop the notion of the independent scales t_0 and T_0 and use only T_0 in the sequel. Note, however, that for short times $t < T_0$, the two functions $R(t)$ and $\ell_B(t)$ scale differently with N. $R(t)$ is always a monotonically decreasing function of N and will be found to decay like N^{-1} for $t < T_0$ in the whole class of local thermal displacement models defined above, while $\ell_B(t)$, by definition, does not depend on N at all. For times t with $\ell_B(t)$ much larger than the microscopic length scales but smaller than R_G, we expect some nontrivial short-time behavior, which for a renormalizable model should be universal. Since T_0 grows with N, while the microscopic scales and $\ell_B(t)$ are independent of N, there is a considerable time range in which short-time universality can be expected.

We now recall some general aspects of the problem and describe our approach. From a theoretical point of view, polymer diffusion in a quenched random medium is a most challenging problem, which is not very well understood. Only a few very simple results concerning static properties of a dilute system of macromolecules have been established rigorously: If a finite number of chains of finite length are free to move within an infinite volume and if the distribution of the random medium is homogeneous in space with finite correlation length, the partition function is self-averaging [4]. If, furthermore, the correlation length of the randomness is microscopic, the disorder average can be carried out by standard means. Dynamic properties in general, however, or even static expectation values in quenched disorder with a finite segment concentration still pose severe unsolved problems. They mainly have been discussed in terms of plausible but somewhat heuristic arguments.

The problems even start with searching for a good and tractable model. This is a simple task only for the polymer part. Being concerned with hopefully universal properties of very long chains, we may ignore all chemical microstructure and model the chain as a sequence of mutually repelling beads or even as a self-repelling space curve (Edwards model). This approach has been most successful in explaining the properties of normal polymer solutions.

To model the quenched disordered medium poses a more complicated problem. Two complementary approaches have been suggested. On the one hand, we may observe that mechanical stability of the medium needs a connected structure of material, which the polymer cannot cross. Its available space therefore is confined to holes that will form a very complex geometrical pattern. The first type of approach tries to deal with the random medium in terms of such purely geometrical or "topological" constraints. On the other hand, the energetic effects then are neglected. Such effects clearly result from the interaction of the polymer with the random material. Furthermore, larger holes allowing for more microscopic configurations of (parts of) the macromolecule, act as entropic traps [5,6]. In coarse graining from a microscopic description of the polymer to the simple model described above, such traps yield a contribution to the local free energy of the effective segments that fluctuates in space. Both the microscopic interactions as well as the entropic traps may be modeled as a quenched random local potential.

It should be clear that a realistic description of the random medium should combine both topological and energetic effects. Unfortunately, at present no such realistic model allowing also for an analytic treatment is known. Static properties generally are discussed within the random potential model. Dynamic properties mostly have been analyzed for topologically defined disorder, which leads to the reptation picture [7,3]. Recently, however, one of us has presented an extensive study of polymer dynamics in the random potential model [2] (this paper will be refered to as I in the following), which will be pursued in the present paper. Starting from a Langevin description of the polymer dynamics and incorporating a local Gaussian distributed random potential as the relevant contribution in the renormalization group (RG) sense, a systematic perturbation theory was formulated. It takes the form of a simultaneous expansion in two couplings, namely, in the excluded volume repulsion u among the polymer segments and in the strength of the disorder, being measured in terms of the second moment v of the Gaussian distribution. The theory was shown to be renormalizable at least to one-loop order and to take along all those short-range effects that are relevant under renormalization and thus govern the large-scale properties. Within the class of random potential models and for sufficiently long chains the results therefore are expected to be universal. They should yield a valid description of experiments, provided the "topological" correlations of the realistic disorder do not play an essential role. As pointed out below, this latter restriction in fact may not be very strong.

Dealing with a renormalizable theory, however, does not necessarily imply the results to take the form of simple power laws. In fact, the analysis has shown that the disorder coupling v does not reach a stable fixed point within the realm of perturbation theory. Our results therefore are formulated as nonlinear crossover functions, not reducing to power laws. The RG allows us to discuss the general nonlinear scaling forms and to determine which combinations of the original parameters appear as scaling variables. The explicit evaluation of our perturbation theory to one-loop order, however, is restricted to very weak disorder on the microscopic scale, which nevertheless should yield the universal behavior in an appropriate parameter range.

Let us now briefly recall our earlier results for the short- and long-time behavior of our model. For long times $t \gg T_0$ normal diffusion of the center-of-mass motion was found, i.e., $R^2(t) = D\,t$. The N dependence of the diffusion constant D was found to be $N^{-1}\,\mathcal{D}(\bar{v}(l_R))$, with $\bar{v}(l_R)$ being the renormalized coupling on the scale l_R and l_R being a scale of the order of the polymer size R_G. Under the simplifying assumption of the effective excluded volume interaction $w = u - v$ being close to the excluded volume fixed point, $\bar{v}(l_R)$ is a unique function of $v\,N^{2-d\nu}$. The N dependence of the diffusion constant is very nonlinear and not of a power law type. The explicit results of the evaluation of the one-loop perturbation theory can be found in [1,2]. The special limit of $t \gg T_0$ will be put into the framework of a general scaling function in the present paper.

The crossover time T_0 in the free theory $u = v = 0$ scales like N^2, leaving ample space for universal short-time behavior dominated by the motion of time blobs $\ell_B(t) \ll \ell_B(T_0) = \mathcal{O}(\sqrt{N})$, but much larger than the microscopic scales. For this universal short-time behavior $t \ll T_0$, two of us had presented some earlier prediction [1], suggesting that $R(t)$ obeys some anomalous power law in t with an exponent depending again on $\bar{v}(\ell_R)$ with the same choice $\ell_R = \mathcal{O}(R_G)$. This would imply some nontrivial N dependence of the anomalous time exponent. However, as pointed out above, the reinvestigation of the analytic expressions in the short-time regime as stimulated by the results of the Monte Carlo simulations also presented in this paper has lead us to identify the blob size $\ell_B(t)$ as another dynamic length scale. We now find that the structure of the analytic results strongly suggests the choice of the renormalized length scale ℓ_R as $\ell_R \sim \ell_B(t)$. Then, in contrast to our earlier work, no recourse to exponentiating logarithmic time divergencies appearing in an ϵ expansion is required. All singularities are eliminated by the appropriate choice of ℓ_R. As a result, we now find analytically and in agreement with the Monte Carlo simulations that in the universal short-time regime the product of the chain length and the mean square displacement of the center of mass $NR^2(t)$ is independent of N. It shows a nontrivial time dependence not in the form of a power law in t. Choosing parameters comparable to those of the Monte Carlo simulation, the analytical results, however, can be numerically fitted by an anomalous power law in t over many decades of t with a surprising accuracy. They are in quantitative agreement with the simulations.

In the long-time regime the same quantity $NR^2(t)$ is linear in t and depends on N only through $\bar{v}(\ell_R)$, where here the choice of $\ell_R = \mathcal{O}(N^\nu \ell)$ is the appropriate one. It thus has a nontrivial and non-power-law dependence on N as recalled above, while the t dependence is trivial.

Qualitatively our results strongly resemble results of computer experiments [8] simulating the motion of a polymer through a quenched random system of topological constraints. This supports the idea [9,10] that energetic disorder or entropic traps strongly can modify the behavior predicted by the reptation model.

Our paper is organized as follows: In Sec. II we define the model and we collect the results from paper I [2] needed in the sequel. In Sec. III we present and analyze in detail the blob picture. In Sec. IV we derive the general form of the scaling laws and Sec. V presents the numerical evaluation of our one-loop results. Section VI is devoted to the Monte Carlo simulations. Section VII summarizes our findings and discusses the range of validity of our results. In the Appendix we derive, for completeness, the renormalization group flow equations used here.

II. DEFINITION OF THE MODEL AND COLLECTION OF SOME PERTURBATIVE RESULTS

A. Model

We describe the configuration of the polymer chain embedded in d-dimensional space by fixing the set $\{\mathbf{r}_j\}$,

$j = 1,\ldots,N$, of vectors giving the positions of the monomers. The potential energy (in units of k_BT) is written as

$$\mathcal{H}\{\mathbf{r}_j\} = \sum_{i=2}^{N} \frac{(\mathbf{r}_i - \mathbf{r}_{i-1})^2}{4\ell^2} + u\ell^d \sum_{1\le i<j\le N} \delta^d(\mathbf{r}_i - \mathbf{r}_j) + \sum_{i=1}^{N} V(\mathbf{r}_i) \; . \tag{2.1}$$

The first term identifies our model as a discrete Gaussian chain of average segment size $\langle(\mathbf{r}_i - \mathbf{r}_{i-1})^2\rangle \approx 2d\ell^2$, ℓ setting the microscopic scale. The second term introduces an excluded volume repulsion among the monomers, of dimensionless strength $u \ge 0$. The one-body potential of the last term is assumed to be a random variable, distributed according to a Gaussian distribution

$$\mathcal{P}_v[V] = \mathcal{N} \exp\left[-\int d^dr \frac{V^2(\mathbf{r})}{2v\ell^d}\right] . \tag{2.2}$$

$\mathcal{N}$ is a normalization constant. The parameter v governs the width of the distribution and will play the role of a coupling constant measuring the strength of the disorder.

Dynamics is introduced via the Langevin equation

$$\frac{\partial}{\partial t}\mathbf{r}_i(t) = \gamma\left[-\nabla_i \mathcal{H}\{\mathbf{r}_j(t)\} + \mathbf{f}_i(t)\right] \quad , \tag{2.3}$$

where ∇_i denotes the gradient with respect to $\mathbf{r}_i(t)$. This equation describes an overdamped motion under the influence of thermal forces $\mathbf{f}_i(t)$ acting on the ith monomer. For these forces the usual white noise distribution is taken

$$\mathcal{P}_f\{\mathbf{f}_i\} = \mathcal{N}' \exp\left[-\frac{\gamma}{4}\sum_{i=1}^{N}\int dt\, \mathbf{f}_i^2(t)\right] . \tag{2.4}$$

As has been discussed in I, this model contains all short-range terms that are relevant according to standard power counting. It further must be recalled that Eqs. (2.1)–(2.4) are formal, needing regularization in intermediate steps of the calculation. Specifically, in the static part (2.1) and (2.2) both the δ-function potential and the local fluctuations of $V(\mathbf{r})$ must be smoothened and in the dynamic part we must discretize the time continuum and also must include some potential confining the center-of-mass motion. Since these aspects do not show up in the final results and since they carefully have been discussed in I, here we do not consider such technicalities any more.

B. Results of unrenormalized perturbation theory

In I the model was evaluated by constructing a generating functional for the correlation functions. This functional may be expanded about the Rouse limit, i.e., the noninteracting ($u = 0$) chain in homogeneous space [$V(\mathbf{r}) \equiv 0$, i.e., $v = 0$]. Here we are interested in the motion of the center of mass

$$\mathbf{R}_{\text{c.m.}}(t) = \frac{1}{N}\sum_{j=1}^{N}\mathbf{r}_j(t) \quad , \tag{2.5}$$

as represented by the mean square distance the polymer moves within time t

$$R^2(t) = \overline{\langle[\mathbf{R}_{\text{c.m.}}(t+t_0) - \mathbf{R}_{\text{c.m.}}(t_0)]^2\rangle} . \tag{2.6}$$

Since we take the system to be in thermodynamic equilibrium, $R^2(t)$ is independent of t_0. It furthermore is independent of the position of the starting value $\mathbf{R}_{\text{c.m.}}(t_0)$, due to the translational invariance of the ensemble $\mathcal{P}_v[V]$.

The first-order result for $R^2(t)$ ("one loop") is found in I, Eq. (7.26):

$$R^2(t) = 2d\Gamma t\left[1 - \hat{v}\,\Gamma\int_0^t d\hat{\tau}\left(1 - \frac{\hat{\tau}}{t}\right) \times \int_0^S \frac{ds_i ds_j}{4}\, D_{ij}(\hat{\tau})^{-3+\epsilon/2}\right] . \tag{2.7}$$

Here the ususal notation $\epsilon = 4 - d$ is introduced and

$$S = N\,\ell^2, \qquad s_i = i\,\ell^2, \qquad s_j = j\,\ell^2,$$
$$\hat{v} = 2(4\pi)^{-d/2} v\,\ell^{-\epsilon}, \qquad \hat{\gamma} = \gamma\,\ell^2, \quad \Gamma = \frac{\gamma}{N} = \frac{\hat{\gamma}}{S} \quad .$$

Throughout this paper we take $t \ge 0$. The result (2.7) is written in dimensional regularization, i.e., assuming $d < 4 (\epsilon > 0)$ and taking the continuous chain limit $\ell \to 0$ with $S, s_i, s_j, \hat{\gamma}, \hat{v}$ (and with a similar variable $\hat{u}$ derived from u) held fixed. This limit simplifies the calculations and suppresses microstructure effects. In particular it sets the microscopic time scale $T_\ell \sim \ell^2/\gamma$ to zero. The function $D_{ij}(\hat{\tau})$ is the counterpart of $\mathcal{D}_{ij}(t)$ [Eq. (1.1)] in a noninteracting theory and derives from the motion of internal segments of a Rouse chain

$$D_{ij}(\hat{\tau}) = \frac{1}{2}\langle[\mathbf{r}_i(\hat{\tau} + t_0) - \mathbf{r}_j(t_0)]^2\rangle_{u,v\equiv 0}$$

[I, Eq. (A.2)]. An explicit form of the one-loop integral will be given below.

Some basic structural aspects of the result (2.7) easily are understood. The leading term $R^2(t) = 2d\Gamma t$ just represents free diffusion. In the absence of the one-particle potential $V(\mathbf{r})$ this is the full result for $R(t)$, since excluded volume forces do not ruin translational invariance and therefore by themselves do not couple to the center-of-mass motion. Any nontrivial effect is due to the presence of the fluctuating potential $V(\mathbf{r})$ and in perturbation theory therefore must involve at least one factor of $\hat{v}$. Thus to one-loop order only a term of order $\hat{v}$ can occur. The random potential exerts forces on the individual monomers. Along the chain the effect of these forces is propagated by the function $D_{ij}(\tau)$, which correlates the motion of a pair of monomers.

We now write down a more explicit form of the one-loop result (2.7). We rescale the variables, introducing

$$T = \frac{\hat{\gamma}}{S^2}\,t, \qquad \tau = \frac{\hat{\gamma}}{S^2}\,\hat{\tau},$$
$$x = \frac{s_i + s_j}{S} - 1, \qquad y = \frac{s_j - s_i}{S\sqrt{\tau}},$$

and we use the results of I, Sec. 7.3 and Appendix A, to find after some algebra

$$R^2(t) = 2d\Gamma t[1 - \hat{v}S^{\epsilon/2}\mathcal{R}_1(T)] \quad , \tag{2.8}$$

$$\mathcal{R}_1(T) = \frac{1}{2}\int_0^T d\tau\, \tau^{-1+\epsilon/4}\left(1-\frac{\tau}{T}\right)\int_0^1 dx \int_0^{x/\sqrt{\tau}} dy \times\left\{y+\sqrt{2}\sum_{\mu=-\infty}^{+\infty}\left[g\left(\sqrt{\frac{2}{\tau}}\left(\mu-\frac{y\sqrt{\tau}}{2}\right)\right)+g\left(\sqrt{\frac{2}{\tau}}\left(\mu-\frac{x}{2}\right)\right)\right]\right\}^{-3+\epsilon/2} \quad , \tag{2.9}$$

$$g(a) = \frac{1}{\sqrt{\pi}}\int_0^1 dz\; e^{-a^2/z^2} \quad . \tag{2.10}$$

This form of the result is particularly useful for a discussion of the short-time regime $T \lesssim 1$, which easily is seen to be dominated by small values of $|\mu|$ in the summation. The limit $T \to 0$ is given by the $\mu = 0$ contribution of the first term in the square brackets of Eq. (2.9).

C. Renormalization

For $\epsilon > 0$, Eq. (2.9) yields a finite result for all $0 \le t < \infty$ and $0 \le S < \infty$. For $\epsilon \to 0$ the one-loop correction develops a pole, the divergence resulting from integration over small distances and short times: $(s_i - s_j)^2 \sim \hat{\tau} \to 0$, i.e., $\tau \to 0, y$ finite. For any $T \neq 0$ we find [cf. I, Eq. (4.30) and Appendix B]

$$S^{\epsilon/2}\mathcal{R}_1(T) \underset{\epsilon\to 0}{=} \frac{I}{\epsilon} + O(\epsilon^0) \quad , \tag{2.11}$$

$$I = \int_0^\infty dy\,[y + g(y)]^{-3} = 3.587\ldots \quad . \tag{2.12}$$

Within dimensional regularization such poles are the remainder of the microscopic structure of the chain. To extract the universal physical behavior, which necessarily is given by finite expressions also for $d = 4$, we must absorb the ϵ poles into a redefinition of the parameters of the theory. We thus write

$$\begin{aligned} \hat{u} &= \bar{u}\ell_R^{-\epsilon}Z_u, \quad \hat{v} = \bar{v}\ell_R^{-\epsilon}Z_v \quad , \\ S &= n_R\ell_R^2 Z_n, \quad \Gamma = \frac{\gamma_R}{n_R}Z_\Gamma \quad . \end{aligned} \tag{2.13}$$

Here ℓ_R is an arbitrary length scale introduced to make the renormalized parameters $\bar{u}, \bar{v}, n_R$ dimensionless. γ_R has dimensions (length)^2/time. The renormalization factors Z_u, etc., are written as power series in $\bar{u}, \bar{v}$ with coefficients depending only on ϵ and chosen to cancel the ϵ poles ("minimal subtraction"). The existence of such a choice, which eliminates the poles from all physical correlation functions, is the highly nontrivial property of a renormalizable theory. Clearly, with the results given here we only can determine Z_Γ to first order, but considering other quantities also the other Z factors have been determined and the one-loop renormalizability of the theory has been established (see I).

The renormalized form of Eq. (2.7) is found by subtracting the pole and replacing all variables by their renormalized counterparts

$$R^2(t) = 2d\frac{\gamma_R}{n_R}t\left[1 + \frac{I}{\epsilon}\bar{v} - \bar{v}n_R^{\epsilon/2}\mathcal{R}_1(T_R) + \mathcal{O}\left(\bar{v}^2, \bar{u}\bar{v}\right)\right]. \tag{2.14}$$

The variable

$$T_R = \frac{\gamma_R}{n_R^2\ell_R^2}\,t \tag{2.15}$$

has a simple interpretation as $T_R \sim t/T_0$ with T_0 discriminating between short- and long-time behavior, as described in the Introduction. Indeed the leading-order result can be written as

$$\frac{1}{2d}\,R^2(t) \;=\; n_R\,\ell_R^2\,T_R \;\sim\; R_G^2\,T_R \quad ,$$

where $R_G^2 \sim n_R\ell_R^2$ is the radius of gyration of the chain evaluated to leading order of renormalized perturbation theory. Note that the result of I, Eq. (7.28), is identical to Eq. (2.14) above, but written in a form adequate for discussing the long-time regime.

To evaluate renormalized results we need a manageable form of the mapping from physical (unrenormalized) parameters to their renormalized counterparts. The formal definition (2.13) cannot be used for that purpose since it involves power series with singular coefficients. However, in renormalization theory one proves that derivatives $\partial\bar{u}/\partial\ln\ell_R$, $\partial\bar{v}/\partial\ln\ell_R$, $\partial\ln n_R/\partial\ln\ell_R$, etc., taken with fixed unrenormalized parameters, show a well behaved perturbation expansion in powers of $\bar{u}, \bar{v}$. By construction the resulting "renormalization group flow equations" relate renormalized theories defined on different scales ℓ_R, but all equivalent to the same unrenormalized theory. Integrating these equations, we find the relation among the renormalized parameters defined on different scales, which we may denote by ℓ_R or $\ell_{R,0}$. We now take $\ell_{R,0}$ to be of microscopic size $\ell_{R,0} = \ell$. On that scale the renormalized parameters can be assumed to be regular

functions of the physical parameters since all the critical nonanalytic behavior is due to fluctuations on scales large compared to ℓ. The flow equations therefore yield $\bar{u}$, etc., as functions of

$$\lambda = \ell/\ell_R \quad , \tag{2.16}$$

with integration constants that are microstructure dependent and are taken as fit parameters depending smoothly on the microscopic physics (for examples see below).

The final step in the evaluation of renormalized perturbation theory then consists in choosing ℓ_R. This is a delicate problem, the solution offered in Sec. III being the essential new theoretical contribution of the present work.

With these general remarks we turn to the form of the renormalization group equations for the problem at hand. This in detail has been discussed in [4] (see also I, Secs. 2.2 and 7.2) and we quote the following results.

(i) The combination

$$\bar{w} = \bar{u} - \bar{v} \tag{2.17}$$

of the interaction constants decouples from the other parameters, obeying an equation of the form

$$-\ell_R \frac{\partial \bar{w}}{\partial \ell_R} = \beta_w(\bar{w}) \quad .$$

Also the flow of n_R

$$-\ell_R \frac{\partial \ln n_R}{\partial \ell_R} = \frac{1}{\nu(\bar{w})}$$

depends on $\bar{w}$ only. Furthermore, these equations are identical to those found in the theory of equilibrium properties of normal polymer solutions. As a result, the functions $\beta_w(\bar{w}), \nu(\bar{w})$ are known to good precision [11]. In particular, for $\epsilon > 0$ there exists a fixed point $\bar{w}^* = \frac{\epsilon}{4} + O(\epsilon^2)$, which for all starting values $\bar{w}_0 > 0$ is reached in the limit $\lambda = \ell/\ell_R \to 0$. (In $d = 3, \bar{w}^* \approx 0.364$ is found from a higher-order calculation.) If we assume that the starting value of $\bar{w}$ is already close to the fixed point $\bar{w} = \bar{w}^*$, the equation for n_R yields

$$n_R = \lambda^{1/\nu} \hat{N} \quad , \quad \hat{N} = c_N \, N \quad , \tag{2.18}$$

where $\nu = \nu(\bar{w}^*) = 0.588\ldots$ in $d = 3$ and $\hat{N}$ is proportional to the bare chain length N. The nonuniversal proportionality constant c_N absorbs the integration constants and depends on the microscopic interactions. For $\bar{w} = \bar{w}^*$ the polymer chain is said to have reached the excluded volume limit, where, for instance, the equilibrium size of an isolated polymer coil in solution scales as $R_G \sim \hat{N}^\nu$. In the following we for simplicity will assume $\bar{w}$ to have reached its fixed point so that the flow of $\bar{w}$ needs no further consideration.

(ii) The flow of the disorder strength $\bar{v}$ can be taken from the theory of solutions containing two different polymer species ("ternary solutions"). For $\bar{w} \equiv \bar{w}^*$ the integrated flow of $\bar{v}$ to a good approximation is found as

$$\bar{v}(\lambda) = \left((s_v \lambda)^{\omega_{12}^*} - \frac{1}{\bar{w}^*} \right)^{-1} \quad , \tag{2.19}$$

where $\omega_{12}^* \approx 0.40$ and

$$s_v^{\omega_{12}^*} = \frac{1}{\bar{v}(1)} + \frac{1}{\bar{w}^*} \quad . \tag{2.20}$$

This result can be extracted from [12], but for completeness we sketch a derivation in the Appendix. [Note a slight change of notation. The couplings $\bar{v}(l)$ and $\bar{v}(l_R)$ from [1,2] and the Introduction are from here on denoted as $\bar{v}(1)$ and $\bar{v}(\lambda)$.]

From Eqs. (2.19) and (2.20) it is obvious that for $\bar{v}(1) < 0$ the coupling $\bar{v}(\lambda)$ for $\lambda \to 0$, i.e., $\ell_R \to \infty$, tends to $-\bar{w}^*$. In the present problem, however, $\bar{v}(1)$ is positive definite, being the second moment of a probability distribution. For $\bar{v}(1) > 0$ the fixed point is not reached, but $\bar{v}(\lambda)$ with decreasing λ leaves the region $\bar{v} \lesssim 1$ where perturbation theory may be trusted. This restricts our explicit calculations to the limit of weak disorder. We assume $\bar{v}(1)$ to be so small that $\bar{v}(\lambda) \lesssim 1$ holds for all values of λ encountered in our evaluation of renormalized perturbation theory.

(iii) The flow of γ_R is specific to the dynamical problem. It has been calculated to one-loop order and the results of I yield (see also the Appendix of the present paper)

$$\gamma_R(\lambda) = (s_v \lambda)^{1/\nu} \left(1 + \frac{\bar{v}(\lambda)}{\bar{w}^*} \right)^{-\sigma/\omega_{12}^*} \tilde{\gamma} \quad , \tag{2.21}$$

where $\tilde{\gamma}$ is proportional to the microscopic segment diffusion constant γ, the proportionality factor being microstructure dependent. The exponent σ takes the value

$$\sigma = \frac{\epsilon}{4} I + O(\epsilon^2) \overset{\epsilon=1}{\approx} 0.90 \quad . \tag{2.22}$$

Since σ is known only to leading order in ϵ, its value certainly is not very precise. We believe that this is the main source of numerical uncertainty of our results. It could be cured only by an extremely tedious higher-order calculation of Z_Γ.

Equations (2.18)–(2.22) define the renormalization group mapping to be used in the following. It should be noted that the simplifying assumption $\bar{w} \equiv \bar{w}^*$ is not essential. It could be relaxed at the price of somewhat more involved calculations. [The flow of $\bar{v}(\lambda)$ would become quite complicated but has been worked out in the Appendix of Ref. [12].] We finally should stress again that all the results given in this section only recall or rephrase previous work.

III. TIME BLOBS AND CHOICE OF THE RENORMALIZED LENGTH SCALE

The renormalized theory is scale invariant, which means that macroscopic quantities, if calculated to all orders, are independent of the arbitrary scale ℓ_R. Approximations based on finite-order perturbation theory, however, in general are not rigorously scale invariant. If, based on low-order perturbation theory, we want to con-

struct a good crossover function that interpolates among qualitatively different behavior in various limits ($t \ll T_0$ or $t \gg T_0$, for instance), then the appropriate choice of ℓ_R is an important question. Ideally ℓ_R should be chosen such that the leading (zero-loop) order of perturbation theory qualitatively yields the correct behavior, higher orders contributing only finite (hopefully small) corrections in all the physical parameter range. In struggling for that goal an identification of the important length scales is essential.

To analyze the problem for the center-of-mass motion of the chain we first consider the long-time regime $t \gg T_0$, where the chain has moved a distance large compared to its radius R_G. In that region the only relevant scale is the radius R_G itself. Identifying $\ell_R \approx R_G$ and taking into account the zero-loop result $R_G^2 \sim \ell_R^2\, n_R$, we find the condition

$$n_R = 1 \quad , \tag{3.1}$$

which implicitly fixes ℓ_R. Underlying that choice is the simple picture that in the long-time limit the polymer coil moves like a Brownian particle. We thus can view it as a single effective segment, showing normal diffusional behavior. The internal structure determines the renormalized diffusion coefficient as a universal quantity. This idea can be and should be checked with the perturbative results. As has been worked out in I, Sec. 7.3, $R^2(t)$ in the long-time limit can be written as

$$R^2(t) = 2d\,\frac{\gamma_R}{n_R}\,t\left[1 - \bar{v}\left(\left(n_R^{\epsilon/2} - 1\right)\frac{I}{\epsilon} + n_R^{\epsilon/2}\mathcal{A}(\infty,\epsilon)\right)\right] , \tag{3.2}$$

where $\mathcal{A}(\infty,\epsilon)$ is a numerical constant of order 1. For $\bar{v} \lesssim 1$ the choice $n_R = O(1)$ therefore guarantees that the one-loop term just yields some finite correction, the dominant behavior being given by the prefactor, which just is the renormalized zero-loop term.

We now turn to the limit $t \ll T_0$. (Recall that the microscopic time scale T_ℓ has been set to zero by taking the continuous chain limit. For a physical chain it must be understood that $T_\ell \ll t \ll T_0$.) Now at such short time differences the segments i and j far apart along the chain move independently. As explained in the Introduction, we thus consider the chain after time t as a sequence of $n_R = n_R(t)$ "time blobs" of spatial size $\ell_B = \ell_R(t)$, defined such that the blobs can be taken as moving independently up to time t. We determine ℓ_B self-consistently on the basis of the zero-loop approximation.

The number of segments in a time blob is N/n_R. Considered as a free chain, such a blob moves according to

$$\langle[\mathbf{R}_{\text{c.m.}}^{(\text{blob})}(t) - \mathbf{R}_{\text{c.m.}}^{(\text{blob})}(0)]^2\rangle \sim \frac{\gamma\, t}{N/n_R} \approx \gamma_R\, t \quad . \tag{3.3}$$

The last equality follows from the relation $\gamma/N = \gamma_R/n_R$ valid to leading order in the presence of the random potential or rigorously true for free chains. Equation (3.3) identifies γ_R as the blob diffusion coefficient. Being of size ℓ_B, this blob will start to "feel" the constraints tying it to its neighbors after it has moved a distance of order ℓ_B. Thus

$$\ell_B = \ell_R(t) = \sqrt{\gamma_R[\ell_R(t)]\; t} \tag{3.4}$$

defines the size of the time blobs. For short times this is the relevant scale, since we should not combine into a single effective segment ℓ_R parts of the chain that essentially move independently of each other.

Before checking this picture with the one-loop results, we consider some consequences. In terms of the center of mass $\mathbf{R}_{\text{c.m.}}^{(j)}$ of the jth blob, the displacement of the total chain can be written as

$$\mathbf{R}_{\text{c.m.}}(t) - \mathbf{R}_{\text{c.m.}}(0) = \frac{1}{n_R}\sum_{j=1}^{n_R}[\mathbf{R}_{\text{c.m.}}^{(j)}(t) - \mathbf{R}_{\text{c.m.}}^{(j)}(0)] \quad .$$

According to the blob picture the displacements $\mathbf{R}_{\text{c.m.}}^{(j)}(t) - \mathbf{R}_{\text{c.m.}}^{(j)}(0)$ are independent random variables obeying Eq. (3.3). This immediately yields

$$n_R^2\overline{\langle[\mathbf{R}_{\text{c.m.}}(t) - \mathbf{R}_{\text{c.m.}}(0)]^2\rangle} \sim n_R\,\gamma_R\,t$$

or

$$R^2(t) \sim \frac{\gamma_R t}{n_R} \quad . \tag{3.5}$$

We thus recover the zero-loop result. From (3.4) we know that ℓ_R is a function of t independent of N, so that $n_R = \lambda(t)^{1/\nu}\hat{N}$, by virtue of Eq. (2.18). In its range of applicability $t \ll T_0$ the blob picture therefore predicts a very simple chain length dependence:

$$R^2(t) \sim \frac{f(t)}{\hat{N}} \quad , \tag{3.6}$$

where the function f depends on t, γ, and disorder strength v. In particular, the limit $\lim_{N\to\infty}[\hat{N}R^2(t)]$ should exist.

It also is of interest to note that the blob picture immediately yields the well known behavior

$$D_{ii}^{1/2}(t) = \left\langle[\mathbf{r}_i(t) - \mathbf{r}_i(0)]^2\right\rangle^{1/2} \sim t^{1/4} \, , \tag{3.7}$$

valid for interior segments of a noninteracting (Rouse) chain in the short-time regime. Recall that this law easily is derived from dimensional analysis in the continuous chain model, if we assume that $D_{ii}(t)$ for $t \ll T_0$ is independent of the total chain length S, but depends only on $\hat{\gamma}$ and t. Since $\hat{\gamma}$ has dimensions (length)^4/time, Eq. (3.7) follows. To derive this result from the blob picture, we consider segment i as part of an appropriate time blob:

$$D_{ii}(t) \sim \ell_B^2 \sim \ell_R^2(t) \sim \gamma_R\, t \quad .$$

For a noninteracting chain the relation $\gamma_R = \gamma\, n_R/N$ holds and the number N/n_R of segments in the time blob is related to ℓ_B via $\ell_B^2 = \ell^2 N/n_R$. Thus

$$\ell_B^2 \sim \gamma \frac{\ell^2}{\ell_B^2} t$$

or

$$D_{ii}^{1/2}(t) \sim (\gamma \ell^2 t)^{1/4} \quad ,$$

which is the desired result.

These considerations qualitatively support the blob idea. The crucial test now is the analysis of the one-loop correction. For $t \ll T_0$, i.e., $T_R \ll 1$, we find from Eq. (2.9)

$$\mathcal{R}_1(T_R) \overset{T_R \to 0}{\longrightarrow} \frac{1}{2} T_R^{\epsilon/4} \int_0^1 d\tau\, \tau^{-1+\epsilon/4}(1-\tau) \times \int_0^\infty dy \left[y + \sqrt{2}\, g\left(\frac{y}{\sqrt{2}}\right)\right]^{-3+\epsilon/2} , \tag{3.8}$$

where we rescaled $\tau \to T_R \tau$ before taking the limit $T_R \to 0$. The integral yields a numerical coefficient singular for $\epsilon \to 0$. Thus

$$\mathcal{R}_1(T_R) \overset{T_R \to 0}{\longrightarrow} \frac{a_0(\epsilon)}{\epsilon} T_R^{\epsilon/4} \quad , \tag{3.9}$$

where it is easily checked that $a_0(0) = I$ [cf. Eq. (2.12)]. Substituting this result into Eq. (2.14), we find

$$R^2(t) \overset{T_R \to 0}{\longrightarrow} 2d \frac{\gamma_R}{n_R} t \left[1 + \bar{v} \left(\frac{I}{\epsilon} - (n_R^2 T_R)^{\epsilon/4} \frac{a_0(\epsilon)}{\epsilon} \right) \right] . \tag{3.10}$$

Choosing now ℓ_R such that the one-loop corrections stay small, we recover the physically motivated blob concept once again, this time on purely mathematical grounds: From Eq. (2.15) we note

$$n_R^2 T_R = \frac{\gamma_R t}{\ell_R^2} \quad , \tag{3.11}$$

so that the identification of ℓ_R with the size of the time blob [Eq. (3.4)] yields $n_R^2 T_R = 1$. As a result, the one-loop correction does not seriously change the character of $R^2(t)$ as found in the zero-loop approximation. Indeed, if $\bar{v}$ would attain a fixed point, the one-loop correction just would numerically change the coefficient of the then resulting anomalous power law. Even in the present case the dominant behavior for $\bar{v} \lesssim 1$ is given by the prefactor in Eq. (3.10). (See Sec. V for the explicit evaluation.) This demonstrates the validity of the blob concept.

Up to now we have considered the choice of ℓ_R in the two limits $t/T_0 \gg 1$ and $t/T_0 \ll 1$. To describe the crossover as function of t, we need to interpolate smoothly among the two prescriptions (3.4) or (3.1). We use the obvious choice

$$\frac{1}{\ell_R^2} = \frac{1}{\gamma_R t} + \frac{1}{\ell_R^2 n_R} \quad , \tag{3.12}$$

reducing to the correct prescriptions in both limits. Clearly we could multiply the terms with numerical factors of order 1, thus changing the relative weight of the two important scales. Such modifications, however, do not seriously influence the numerical results and certainly are irrelevant at the present stage of the theory. Equation (3.12) is the last piece needed for the evaluation of $R^2(t)$ for arbitrary $t \gg T_\ell$.

It should be noted that the discussion as given here closely follows the (most successful) analysis of the crossover from the dilute to the semidilute regime occurring for static properties of polymer solutions [13]. For that problem ℓ_R must be chosen to smoothly interpolate among R_G (dilute limit) and the size of the concentration blob (semidilute limit).

IV. GENERAL SCALING BEHAVIOR AT THE EXCLUDED VOLUME FIXED POINT

Independent of the one-loop approximation, the renormalization group implies scaling laws, stating that observables can depend only on certain combinations of their variables. We now first will discuss these laws before deriving them below.

Provided the system has reached the excluded volume fixed point, the general scaling law for $R^2(t)$ reads

$$\frac{R^2(t)}{2d\tilde{\ell}^2} = \frac{\tilde{t}}{\tilde{N}} \mathcal{R}(\tilde{N}, \tilde{t}) \quad . \tag{4.1}$$

$\mathcal{R}(\tilde{N}, \tilde{t})$ is a universal function, independent of the strength of the disorder. The latter is absorbed into the variables $\tilde{N}, \tilde{t}, \tilde{\ell}$, which are proportional to $\hat{N} = c_N N, t, \ell$, respectively. It is only in the proportionality factors that the starting value $\bar{v}(1)$ of the disorder coupling and thus the microscopic disorder strength shows up. The general form of these factors will be derived below. Specifically in the limit of weak disorder $\bar{v}(1) \to 0$ we find the simple form

$$\begin{aligned} \tilde{N} &= \bar{v}(1)^{1/(2-\nu d)} \hat{N} \quad , \\ \tilde{t} &= \bar{v}(1)^{(2\nu+1)/(2-\nu d)} \frac{\gamma}{\ell^2} t \quad , \\ \tilde{\ell} &= \bar{v}(1)^{-\nu/(2-\nu d)} \ell \quad . \end{aligned} \tag{4.2}$$

(Note that, accordingly, $\tilde{N}$ and $\tilde{t}$ take very small and $\tilde{\ell}$ takes very large numerical values.)

From the general scaling form (4.1) we can derive different limits for the short- or long-time regime.

(i) In the long-time regime of $t \to \infty$ and N fixed, we find normal diffusion, i.e., $R^2(t)/t$ becomes independent of t. The so defined diffusion constant, which has been discussed in more detail in I, Sec. 7.3, can be expressed by the scaling function (4.1) as

$$\frac{R^2(t)}{2d\,\tilde{\gamma} t} = \frac{\mathcal{R}(\tilde{N}, \infty)}{\tilde{N}} \quad \text{for} \quad t \gg T_0 \tag{4.3}$$

($\tilde{\ell}^2 \tilde{t} = \tilde{\gamma} t$, see below). Choosing the time scale as $1/\tilde{\gamma}$, we thus get the diffusion constant as a universal func-

tion of $\tilde{N}$ only. $\tilde{N}$ is in general given by (4.12) below or specifically in the limit of $\bar{v}(1) \to 0$ (4.2) as $\tilde{N}^{\alpha} = \bar{v}(1)\,\hat{N}^{\alpha}$, $\alpha = 2 - d\nu$.

(ii) The short-time limit is given by $T_R \sim 1/n_R^2 \to 0$ or $n_R \to \infty$. Furthermore, as has been discussed in Sec. III, the blob picture, as supported by our one-loop results, predicts that $NR^2(t)$ exists in that limit. For this expression the short-time limit is thus equivalent to taking $\tilde{N} \to \infty$ for $\tilde{t}$ fixed. In terms of the scaling function this implies that

$$\frac{\hat{N}\,R^2(t)}{2d\,c_\ell^2\ell^2} = \tilde{t}\,\mathcal{R}(\infty,\tilde{t}) \quad \text{for} \quad t \ll T_0 \tag{4.4}$$

($c_\ell = s_v^{1+1/2\nu}$, see below). This is the more precise version of Eq. (3.6). Accordingly, if measuring the length scale in units of $c_\ell \ell$, $\hat{N}R^2(t)$ is a function of $\tilde{t}$ only.

(iii) Note, finally, that the crossover regimes $t \approx T_0$ for different values of $\tilde{N}$ in general cannot be shifted onto each other. We thus find a one-parameter family of curve shapes at $t \approx T_0$, which are parametrized by $\tilde{N}$.

We now sketch the derivation of the basic result (4.1).

From Sec. II we take the general result

$$\frac{R^2(t)}{2d} = \frac{\gamma_R\,t}{n_R}\,\hat{\mathcal{R}}(n_R, T_R, \bar{v}) \quad , \tag{4.5}$$

valid at the excluded volume fixed point. The integrated RG equations can be written (cf. the Appendix) as implicit equations for the renormalized disorder strength $\bar{v}(\lambda)$ on the scale $\ell_R = \ell/\lambda$,

$$F_v(\bar{v}(\lambda)) = s_v\,\lambda \quad , \tag{4.6}$$

or for the renormalized blob diffusion constant

$$\gamma_R(\lambda) = (s_v\,\lambda)^{1/\nu}\,F_\gamma(\bar{v}(\lambda))\,\tilde{\gamma} \quad , \tag{4.7}$$

where

$$s_v = F_v(\bar{v}(1)) \quad , \tag{4.8}$$

$$\tilde{\gamma} = \gamma_R(1)\,F_\gamma^{-1}(\bar{v}(1))\,s_v^{-1/\nu} \quad . \tag{4.9}$$

The functions F_v and F_γ depend only on the "running coupling" $\bar{v}(\lambda)$. From Eq. (3.12) we conclude

$$n_R^2\,T_R = \frac{\gamma_R\,t}{\ell_R^2} = \frac{n_R}{n_R - 1} \quad , \tag{4.10}$$

where $n_R \to 1$ yields the long-time limit $T_R \to \infty$, whereas the short-time limit $T_R \to 0$ is found for $n_R \to \infty$. Now, from Eq. (4.6) $\bar{v}(\lambda)$ depends only on $s_v\lambda$, a combination that also can be introduced into the expression for n_R:

$$n_R(\lambda) = (s_v\,\lambda)^{1/\nu}\,\tilde{N} \quad , \tag{4.11}$$

$$\tilde{N} = s_v^{-1/\nu}\hat{N} \quad . \tag{4.12}$$

[Recall that $\hat{N} = c_N N$ (2.18) with the nonuniversal microstructure-dependent constant c_N.] Combining these results, we find the general form

$$\frac{R^2(t)}{2d} = \frac{\tilde{\gamma}\,t}{\tilde{N}}\,\breve{\mathcal{R}}(\tilde{N}, s_v\,\lambda) \quad . \tag{4.13}$$

The variable $s_v\lambda$ can be expressed in terms of $\tilde{t}$ and $\tilde{N}$ by combining Eqs. (4.10), (4.7), and (4.11)

$$\frac{(s_v\,\lambda)^{1/\nu}\,\tilde{N}}{(s_v\,\lambda)^{1/\nu}\,\tilde{N} - 1} = (s_v\,\lambda)^{2+1/\nu}\,F_\gamma(\bar{v}(\lambda))\,\tilde{t} \, , \tag{4.14}$$

where

$$\tilde{t} = \frac{\tilde{\gamma}}{s_v^2\ell^2}\,t \tag{4.15}$$

again absorbs some nonuniversal microstructure. We thus can write Eq. (4.13) as

$$\frac{R^2(t)}{2ds_v^2\ell^2} = \frac{\tilde{t}}{\tilde{N}}\,\mathcal{R}(\tilde{N},\tilde{t}) \quad ,$$

which reduces to Eq. (4.1) upon introducing the notation

$$\tilde{\ell} = s_v\,\ell \quad . \tag{4.16}$$

In the limit of weak disorder we find (cf. the Appendix) $s_v = \bar{v}(1)^{-\nu/(2-\nu d)}$ and $s_v^{1/\nu}\,\tilde{\gamma} = \gamma$, so that Eqs. (4.12), (4.15), and (4.16) reduce to Eq. (4.2).

The form (4.1) is most appropriate for our subsequent discussion. We may note, however, that we can eliminate $\tilde{\ell}^2$ in favor of the radius of gyration R_G^2. From Eqs. (4.12) and (4.16) we find

$$\tilde{\ell}^2\tilde{N}^{2\nu} = \ell^2\hat{N}^{2\nu} \quad ,$$

where the right-hand side can be shown to equal R_G^2, up to a constant coefficient. Thus the scaling law can also be written as

$$\frac{R^2(t)}{R_G^2} = \frac{\tilde{t}}{\tilde{N}^{1+2\nu}}\,\mathcal{R}'(\tilde{N},\tilde{t}) \quad ,$$

a form that, however, is not very practical in the short-time limit.

V. NUMERICAL EVALUATION OF THE ONE-LOOP APPROXIMATION IN THREE DIMENSIONS

We here evaluate our results directly in three dimensions. Introducing a parameter

$$\tilde{\lambda} = s_v\,\lambda \quad , \tag{5.1}$$

we write Eqs. (4.11) and (2.19) as

$$n_R = \tilde{\lambda}^{1.70}\tilde{N} \quad , \tag{5.2}$$

$$\bar{v} = (\tilde{\lambda}^{0.40} - 2.747)^{-1} \quad , \tag{5.3}$$

where we used $1/\nu = 1.70$, $\omega_{12}^* = 0.40$, and $1/\bar{w}^* = 2.747$. Furthermore from Eq. (4.10)

$$T_R = \frac{1}{n_R^2}\frac{1}{1 - 1/n_R} \quad . \tag{5.4}$$

The scaled time follows from Eqs. (4.14) and (A13)

$$\tilde{t} = \frac{\tilde{\lambda}^{-2}\tilde{N}}{\tilde{\lambda}^{1.70}\tilde{N}-1} F_\gamma^{-1}(\bar{v}) \quad ,$$
$$F_\gamma(\bar{v}) = (1+2.747\bar{v})^{-2.25} \quad , \qquad (5.5)$$

where we used $\sigma/\omega_{12}^* \approx 0.90/0.40$. We finally rewrite $R^2(t)$, Eq. (2.14), in terms of scaled variables

$$\frac{R^2(t)}{2ds_v^2\ell^2} = \frac{\tilde{t}}{\tilde{N}} F_\gamma(\bar{v}) \left[1 + I\bar{v} - \bar{v}n_R^{1/2}\mathcal{R}_1(T_R)\right] \quad .$$

Comparing to Eq. (4.1) we thus find the one-loop expression for the universal scaling function

$$\mathcal{R}(\tilde{N},\tilde{t}) = (1+2.747\bar{v})^{-2.25} \times\{1+\bar{v}[3.587 - n_R^{1/2}\mathcal{R}_1(T_R)]\} \quad . \qquad (5.6)$$

$\mathcal{R}_1(T_R)$ is given by Eq. (2.9), $\epsilon = 1$, an expression that has to be evaluated numerically.

The results considerably simplify in the short-time limit $T_R \to 0$, i.e., $\tilde{N} \to \infty$. Then $\mathcal{R}(\tilde{N},\tilde{t}) \to \mathcal{R}(\infty,\tilde{t})$, where

$$\mathcal{R}(\infty,\tilde{t}) = (1+2.747\bar{v})^{-2.25}\,[1+0.569\ \bar{v}] \quad . \qquad (5.7)$$

This result has to be evaluated with Eq. (5.3) and with

$$\tilde{t} = \tilde{\lambda}^{-3.70}\ (1+2.747\ \bar{v})^{2.25} \quad . \qquad (5.8)$$

Figures 1 and 2 show the results in the short-time limit. We plotted the scaling function $\mathcal{R}(\infty,\tilde{t})$ or the "effective exponent"

$$\chi := \frac{\partial \ln R^2(t)}{\partial \ln t} \qquad (5.9)$$

against $\log_{10}\tilde{t}$ in the renormalized zero-loop (broken line) or the one-loop (full and dotted line) approximation for the scaling function, i.e., neglecting or taking along the contribution $0.569\ \bar{v}$ in Eq. (5.7). It is clearly seen that the dominant effect is due to the RG mapping. The analytic corrections of the renormalized loop expansion for the scaling function do not introduce dramatic changes. Thus the blob picture seems to be a valid concept also with regard to quantitative calculations. As Fig. 1 shows, $\mathcal{R}(\infty,\tilde{t})$ smoothly decreases with increasing $\tilde{t}$. For $\tilde{t}\to\infty$ it certainly will approach $\mathcal{R}(\infty,\tilde{t}\to\infty)=0$, but the precise behavior in that limit cannot be deduced from the present weak coupling approximation. The effective exponent χ in the range $\bar{v} \lesssim 1$ decreases from 1 to about 0.7. The strength of that decrease is somewhat sensitive to the exponent σ, Eq. (2.22). If for σ we would use the

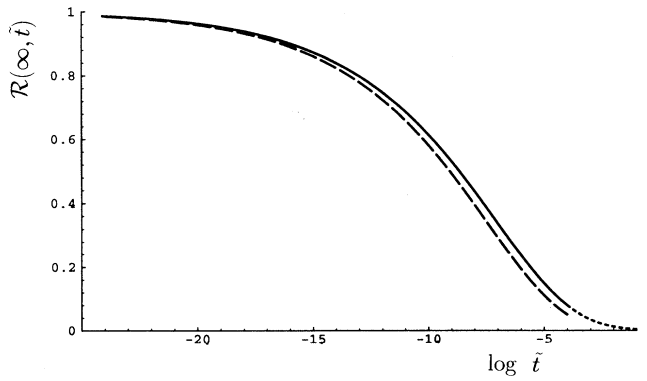

FIG. 1. Scaling function $\mathcal{R}(\tilde{N},\tilde{t})$ in the short-time limit $\tilde{N}=\infty$ as function of $\log_{10}\tilde{t}$. The full line gives the one-loop result, evaluated up to $\bar{v}(\lambda)=1$. The dotted extension covers the interval $1<\bar{v}(\lambda)<10$. The broken line is the renormalized zero-loop result for $\bar{v}(\lambda)\le 1$.

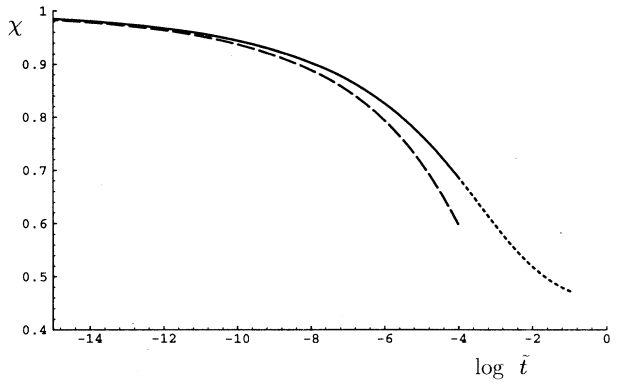

FIG. 2. Effective exponent χ from Eq. (5.9) as a function of $\log_{10}\tilde{t}$. The full, dotted, and broken lines are as in Fig. 1.

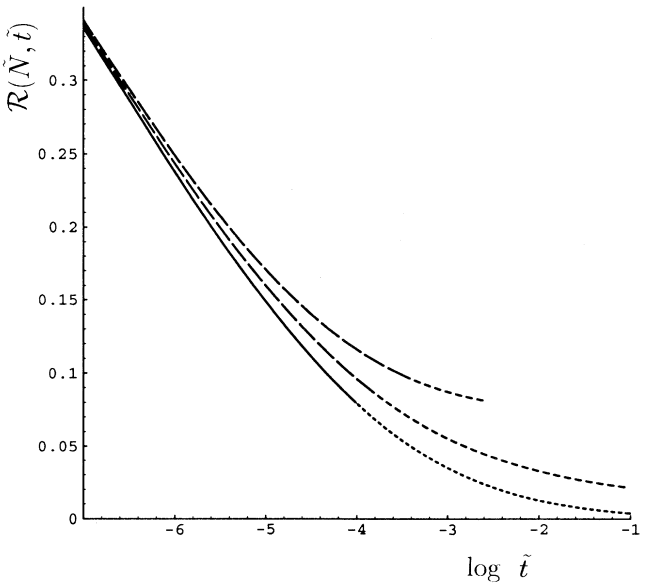

FIG. 3. Scaling function $\mathcal{R}(\tilde{N},\tilde{t})$ as a function of $\log_{10}\tilde{t}$. Full curve, short-time limit ($\tilde{N}=\infty$); broken curves, $\tilde{N}=0.01$ and 0.005 (from below). The dotted extensions represent the region $1<\bar{v}(\lambda)<10$. Only the range where the curves split visibly is shown.

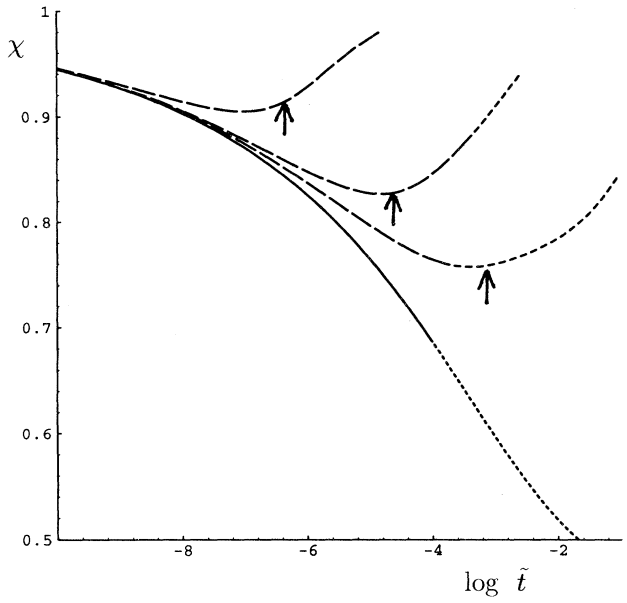

FIG. 4. Effective exponent $\chi(\tilde{N},\tilde{t})$ as function of $\log_{10}\tilde{t}$. Full curve, $\tilde{N}=\infty$; broken curves, $\tilde{N}=0.01$, 0.005, and 0.001 (from below). The arrows give the points $T_R=1$.

approximation $\sigma \approx \bar{w}^* I$, Eq. (A14), with $\bar{w}^* = 0.364$, then the effective exponent would reach a value 0.5 at $\bar{v} \approx 1$. As we mentioned before, this uncertainty of σ seems to be the most serious feature limiting the quantitative accuracy of our results. This is in keeping with experience from other crossover calculations where it is found that a good representation of the RG mapping is the most important ingredient.

Going away from the short-time limit, in Figs. 3 and 4 we have plotted $\mathcal{R}(\tilde{N},\tilde{t})$ or the effective exponents for some values $\tilde{N}<\infty$ in the one-loop approximation. For

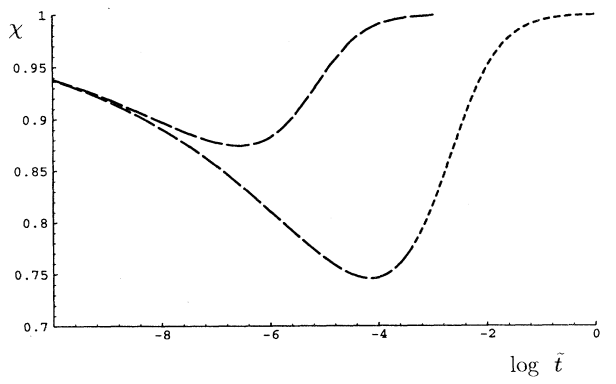

FIG. 5. Effective exponent in renormalized zero-loop approximation as a function of $\log_{10}\tilde{t}$. $\tilde{N}=0.005$ and 0.001 (from below).

finite $\tilde{N}$, $\mathcal{R}(\tilde{N},\tilde{t})$ tends to a finite value $0<\mathcal{R}(\tilde{N},\infty)<1$, which determines the asymptotic diffusion coefficient. Consequently, the effective time exponent of $R^2(t)$, after passing through a minimum, has to approach the value of 1 again. These effects clearly are seen. The minima in Fig. 4 are close to $T_R=1$, which thus sets the scale of the crossover. For smaller times the curves approach the limiting short-time behavior. For large times the curves $\tilde{N}=0.001$ and 0.005 are cut off at $T_R=9$, since for purely technical reasons we did not evaluate $\mathcal{R}_1(T_R)$ for $T_R>9$. [The expression (2.9) is not appropriate for large T_R, where we should switch to another representation of the summation over the Rouse modes; see I.] Figure 5 shows the effective exponent evaluated in zero loop, where the only restriction is on the size of $\bar{v}$. Taking into account the scales of Figs. 4 and 5, it is clear that an experiment over a restricted t range (three decades, for instance) will closely simulate an anomalous power law.

We finally recall that $T_R=1$ roughly corresponds to $R^2(t)=R_G^2$, i.e., $t=T_0$. This relation is not strict, however, and furthermore the asymptotic diffusional regime only sets in for $t \gg T_0$. Clearly, the chain after leaving its original volume occasionally may return, so that it loses memory of its original position only for $t \gg T_0$. These memory effects will increase with increasing disorder.

VI. MONTE CARLO SIMULATIONS

A. Model and simulation techniques

The Gaussian distributed random media has been constructed as follows. Consider a cube of linear dimension L. A simple cubic lattice of lattice spacing a is constructed out of this cube such that $L=80a$. The random medium is introduced by attributing to each of the 80^3 cells a potential $V_{\mathbf{n}}$, where $\mathbf{n}=(n_1,n_2,n_3)\in\{1,2,\ldots,80\}^3$ denotes the position of the cell. $V_{\mathbf{n}}$ is chosen according to a Gaussian distribution $\mathcal{P}_{\mathrm{MC}}[V_{\mathbf{n}}] = \mathcal{N}\exp\left[-\frac{1}{2}V_{\mathbf{n}}^2/v_{\mathrm{MC}}^2\right]$, i.e., $v_{\mathrm{MC}}^2 \propto v$, with v introduced in Eq. (2.2).

Numerically, the Gaussian distribution is generated in the following way. First a cut-off $|V_{\mathbf{n}}|\le C$, $C=\sqrt{2\,v_{MC}^2\,\ln 10^6}$, is introduced. It is chosen such that the weight of the neglected tails of the Gaussian distribution is $2\int_C^\infty dV_{\mathbf{n}}\,\mathcal{P}_{\mathrm{MC}}[V_{\mathbf{n}}] = \mathcal{O}(10^{-7})$. This is to be compared with the number of independent potentials in the sample $80^3 \approx 5\times 10^5$. The cutoff C, therefore, in our finite volume is negligible. The distribution is then further generated from random numbers η, which are equally distributed on the interval $[0,1]$: In the first step, $V_{\mathbf{n}}$ is chosen equally distributed on the interval $[0,C]$ by $V_{\mathbf{n}}=C\,\eta_1$. Then this value $V_{\mathbf{n}}$ is tested against a second random number η_2, and if $\exp\left[-\frac{1}{2}V_{\mathbf{n}}^2/v_{\mathrm{MC}}^2\right]\ge\eta_2$, it is admitted. Otherwise, a new $V_{\mathbf{n}}$ is generated from a new η_1 and the process is repeated. In a last step the admitted $V_{\mathbf{n}}$'s become $-V_{\mathbf{n}}$, if $\eta_3<1/2$, i.e., with probability 1/2. (An alternative way to generate the positive branch of the Gaussian distribution without introducing a cutoff would be to solve $\mathrm{erf}[V_{\mathbf{n}}/\sqrt{2\,v_{\mathrm{MC}}^2}\,]=\eta$ numerically for

$V_{\mathbf{n}}$, where η is equally distributed in $[0,1]$ and erf is the error function. The negative values of $V_{\mathbf{n}}$ then again are generated by reversing the sign of $V_{\mathbf{n}}$ with probability $1/2$. This latter prescription is found by mapping intervals of η or $V_{\mathbf{n}}$ of the same probability weight of the two distributions onto each other.) Discussing these details, it should be noted that we finally aim at seeing universal properties, which should not depend on the specific potential distribution.

The polymer chain is introduced off lattice and self-repelling. It is modeled as the "pearl-necklace" chain [14] of N hard spheres of diameter $h = 0.8a$, which are jointed together by $N-1$ rigid links of length $l = a$. Chain lengths $N = 40$, 80, and 160 are used in the final evaluation. The chain conformations are generated by using the conventional kink-jump technique: A chain configuration is changed locally by trying rotations of two successive links around the axis joining their end spheres by an angle ϕ chosen randomly from the interval $(-\Delta\phi, \Delta\phi)$. The parameter $\Delta\phi$ is chosen arbitrarily. If an end sphere of the chain is chosen, the terminal link is rotated to a nearby position by specifying two randomly chosen angles (ϕ, ψ) in three dimensions, with $\cos\theta$ being equally distributed in the interval $-1 < \cos\theta < 1$. All rotations that lead to an overlap with any other sphere of the chain (self-excluded volume) have been rejected. When such a rejection takes place, we follow the procedure of the dynamical Monte Carlo method by retaining the old conformation and counting it as the new conformation. We also reject in the same manner configurations where the centers of two beads come to sit in the same cell and thus experience the same potential. This has been done because the disorder on one hand effects the dynamics, Eq. (2.21), and, on the other hand, modifies the starting value of the effective coupling constant, Eq. (2.17), eventually leading to the collapse of the chain for $v > u$. In order to suppress the latter effect, we do not allow occupancy of the same potential by two beads at the same time. This procedure increases the effective hard core volume of the beads. The effect on the simulation data evaluated in the present paper is a simple shift of the time scale.

The interaction of the polymer with the random Gaussian potential has been included in the Monte Carlo simulations using the standard Metropolis criterion. The local displacement of bead i of the polymer chain from position $\mathbf{r}_i$ to position $\mathbf{r}_i'$ is accepted if

$$\exp[V_{\mathbf{n}} - V_{\mathbf{n}'}] > \eta, \tag{6.1}$$

where η is equally distributed in [0,1], and where the center of polymer bead i has moved from $\mathbf{r}_i$ in the local cell $\mathbf{n}$ to $\mathbf{r}_i'$ in another or the same cell $\mathbf{n}'$.

We have simulated the mean-square displacement of the center of mass $R^2(t)$ and also

$$g(t) = \overline{\langle\{[\mathbf{r}_{N/2}(t) - \mathbf{R}_{\text{c.m.}}(t)] - [\mathbf{r}_{N/2}(0) - \mathbf{R}_{\text{c.m.}}(0)]\}^2\rangle}\ , \tag{6.2}$$

a standard function of such simulations. $g(t)$ measures the internal relaxation of the chain, more specifically, the temporal decay of the orientation of the vector between the middle bead and the center of mass. In addition, we have measured the radius of gyration. The time t is measured in units of the Monte Carlo time unit, which corresponds to N attempted moves.

The averaging over the quenched potential has been performed by ensemble averaging as well as by trajectory averaging. Given a potential V, the trajectory average is performed as

$$\langle R^2(t)\rangle_V = \frac{\sum_{\tau>\tau_0}[\mathbf{R}_{\text{c.m.}}(t+\tau)_V - \mathbf{R}_{\text{c.m.}}(\tau)_V]^2}{\sum_{\tau>\tau_0} 1}, \tag{6.3}$$

after a sufficient equilibration time τ_0 from the (nonequilibrium) start configuration. Averaging over a sufficiently long trajectory in a given potential, V, reduces the need of ensemble averaging to three to eight different realizations of V, depending on the value of v_{MC}. As a result, for small t the trajectory averaging is quite efficient, while for large t both poor trajectory averaging and the periodic boundary conditions lead to a larger scatter of the data.

B. Typical results

For $v_{\text{MC}} = 0.8$ and $N = 40$ the data covering a particularly large range of time are shown in Fig. 6. Considering first $g(t)$, we note that after some initial increase it saturates at a value $g(t) \approx R_G^2$. This is the generic behavior, found also in the absence of the disorder potential. $g(t)$ levels off at $t \approx 10^4$, which coincides with the time T_0 the chain needs for moving a distance of order R_G. We conclude that the presence of the disorder does not qualitatively change the internal relaxation of the chain, except for the change of the overall time scale.

We now turn to the center-of-mass motion. Measuring time in Monte Carlo (MC) time units, we find that after some initial regime $t \lesssim T_\ell \lesssim 5$ of free diffusion, the motion of the chain slows down, simulating a power law $R^2(t) \sim t^\chi$, $\chi \approx 0.8$, over several decades of t. Crossover to the diffusional long-time behavior occurs for $t \gtrsim 10^5$, i.e., much later than T_0. These results look most similar to those of Ref. [6], where a quite different type of disorder has been used. We will discuss this observation further in Sec. VII.

More results taken in the intermediate time regime $T_\ell \ll t \lesssim 10\ T_0$ are shown in Fig. 7. Again, we note

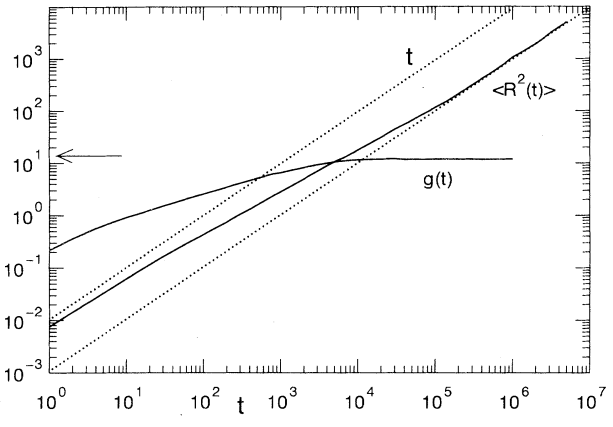

FIG. 6. Doubly logarithmic plot of Monte Carlo data for $R^2(t)$ and $g(t)$. $N = 40$ and $v_{MC} = 0.8$. The arrow points to the value of R_G^2. t is measured in units of MC time. Lengths are measured in units of the size of the disorder cells.

that for at least three decades the data seem to follow a power law $R^2(t) \sim t^\chi$, where the exponent clearly decreases with increasing disorder: $v_{MC} = 0.4$, $\chi \approx 0.96$ and $v_{MC} = 0.6$, $\chi \approx 0.88$. However, no N dependence of χ is visible except that with increasing N the curves simply are shifted downward. Sizeable fluctuations are visible in these curves. This is an artifact due to insufficient averaging over the disorder. It could be suppressed only by averaging over more samples. With our averaging procedure these sample-dependent fluctuations become more pronounced with increasing t. This ultimately restricts the time range of our measurements.

We also measured the radius of gyration to check whether we are close to the excluded volume limit. We found values $N = 40$, $R_G^2 \approx 15.5$; $N = 80$, $R_G^2 \approx 37.0$; and $N = 160$, $R_G^2 \approx 91.7$, with no significant variation with disorder strength. This feature may reflect the fact that we did not allow for multiple occupancy of the same potential cell by polymer beads, as discussed above. Extracting from these data an effective exponent $\nu_{\text{eff}} = \partial \ln R_G / \partial \ln N$, we find $\nu_{\text{eff}} \approx 0.63$, somewhat larger than the asymptotic excluded volume value $\nu \approx 0.59$. This indicates that for our model chain the excluded volume is somewhat large. Indeed, it is known [15] that in the absence of the random potential a pearl-necklace chain most rapidly approaches the excluded volume limit for $h/\ell \approx 0.5$ (h is the diameter of the beads, ℓ the length of the links). Since we have compensated the effective attraction generated by the potential fluctuations (2.17) by choosing $h/\ell = 0.8$ and by not allowing two beads to be subjected to the same potential at the same time, we have overcompensated the effect and work now on the "strong coupling" side of the excluded volume problem. The measured value $\nu_{\text{eff}} \approx 0.63$ suggests that the renormalized excluded volume coupling $\bar{w}$ exceeds its fixed point value by about 20–30 % [16]. In view of the other uncertainties both in theory and in the simulations this seems tolerable.

C. Comparison among theory and data

According to our theory, see (4.4), the product $NR^2(t)$ in the short-time regime should be independent of N. To test this prediction, in Fig. 8 we show a doubly logarithmic plot of $NR^2(t)$ against t, for three values of v_{MC}. For each v_{MC} the data for three chain lengths $N = 40$, 80, and 160 are included. Within their fluctuations, data for given v_{MC} but different N trace out the same curve, thus confirming the blob picture. Indeed, no statistically significant splitting of the curves is found even for times somewhat larger than T_0, which for all cases considered here falls into the range $3 \times 10^3 \lesssim T_0 \lesssim 5 \times 10^4$. To

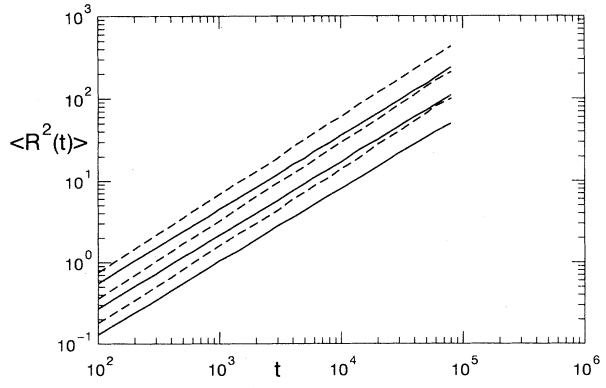

FIG. 7. Doubly logarithmic plot of Monte Carlo data for $R^2(t)$. Dotted lines, $v_{MC} = 0.4$; full lines, $v_{MC} = 0.6$. For each set of lines $N = 40$, 80, and 160 (from above). Units are as in Fig. 6.

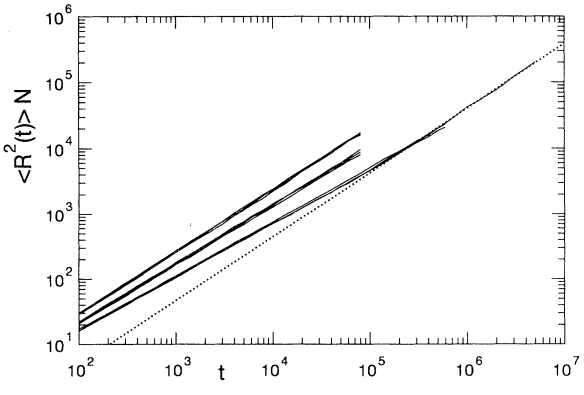

FIG. 8. Doubly logarithmic plot of the Monte Carlo data for $NR^2(t)$. $v_{MC} = 0.4$, 0.6, and 0.8 (from above). For each v_{MC} the results for $N = 40$, 80, and 160 are superimposed. The dotted line represents normal diffusion [$NR^2(t) \propto t$]. Units are as in Fig. 6.

clearly detect the effect of changing N, we would need much improved statistics in the disorder average and we would have to measure for much longer times.

We next show that the theory is consistent with these findings also on the quantitative level. Figure 9 shows $\log_{10}[\tilde{N}\ \mathcal{R}(\tilde{N},\tilde{t})]$ as function of $\log_{10}\tilde{t}$ in the one-loop approximation, where $2d\tilde{t}\mathcal{R}(\tilde{N},\tilde{t}) = \tilde{N}R^2(t)/\tilde{\ell}^2$; cf. Eq. (4.1). We chose two values $\tilde{N} = 0.02$ and 0.08, spanning a range of a factor 4, in accordance with the computer experiment. We included the data for $v_{\rm MC} = 0.6$ and $\tilde{N} = 80$, shifted to bring them close to the theoretical curve. As is clearly illustrated, we can choose $\tilde{N}$ such that the theory simulates the observed effective power law, the splitting according to N being clearly detectable only beyond the range covered by the experiment. Thus both experiment and theory agree that the scaling behavior $NR^2(t) \sim f(t)$, which should rigorously be valid for $t \ll T_0$, to a good approximation extends to $t \sim T_0$. Similar plots for the other values of $v_{\rm MC}$ are not reproduced here.

We finally consider the effective exponent $\chi(t) = \partial \ln R^2(t)/\partial \ln t$, as measured in the computer experiment $v_{\rm MC} = 0.8$ and $N = 40$, which covers a particularly large time interval. Figure 10 shows the result. Numerically differentiating the data we clearly magnify the scatter and in Fig. 10 we see large fluctuations related to the poor disorder average: The chain occasionally gets trapped by large disorder fluctuations. The general trend, however, nicely agrees with the theory. In particular, the depth

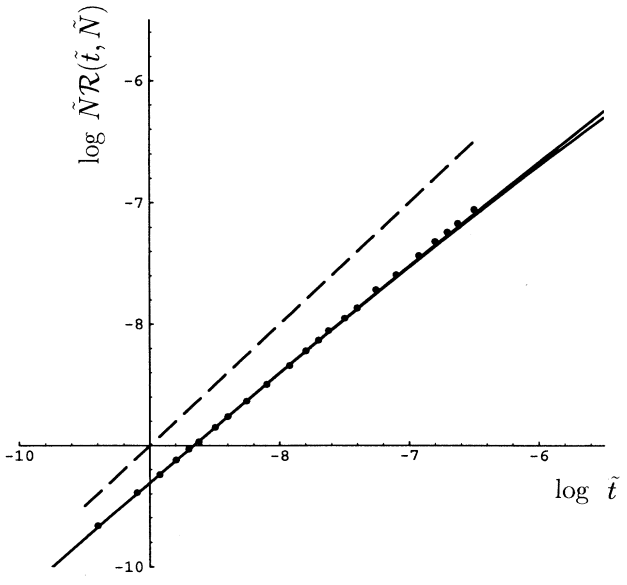

FIG. 9. $\log_{10}\tilde{N}\,\mathcal{R}(\tilde{N},\tilde{t})$ as a function of $\log_{10}\tilde{t}$. Full lines, theory, $\tilde{N} = 0.002$ (upper curve) and $\tilde{N} = 0.008$ (lower curve); broken line, normal diffusion. The MC data for $v_{\rm MC} = 0.06$ and $N = 80$ are brought on top of the theoretical curve by adjusting the nonuniversal scales of $NR^2(t)$ and t. No special effort was made to search for an optimal fit.

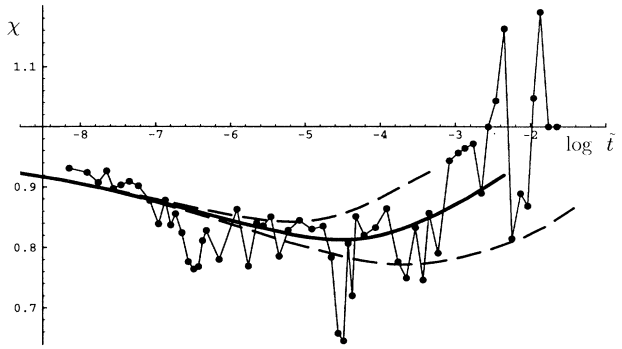

FIG. 10. Effective exponent χ as function of $\log_{10}\tilde{t}$. Data for $v_{\rm MC} = 0.8$ and $N = 40$. The points are connected by lines to guide the eye. Theory, $\tilde{N} = 0.006$ (thick curve), $\tilde{N} = 0.004$ (upper broken curve), and $\tilde{N} = 0.009$ (lower broken curve).

and the width of the valley are well reproduced. It must be noted, however, that we have plotted data starting with very short times. So we cannot exclude the possibility that the data for the first decade of values $\tilde{t}$ are influenced by nonuniversal short-time effects.

VII. DISCUSSION AND CONCLUSIONS

Some qualitative features of the present results are to be expected generally without recourse to any specific model: For microscopic times $\mathcal{O}(T_\ell)$ the chain does not feel the disordered environment and moves freely. As time increases, the motion is slowed down, and for $t \gg T_0$, it again shows normal diffusion, but with a reduced diffusion coefficient. In terms of the effective exponent $\chi(t) = \partial \ln R^2(t)/\partial \ln t$ this implies that χ tends to 1 for $t \to 0$ or $t \to \infty$, but passes through a (positive) minimum at intermediate times.

The present work adds a number of important specifications to this general picture. We first of all note the law $R^2(t) \sim f(t)/N$, holding for macroscopic but short times $T_\ell \ll t \ll T_0$, i.e., in the universal short-time regime. Though this law is a result of the analysis within our specific model, we may invoke the blob picture to argue that it is of general validity. The upper bound of that regime is given by T_0, as long as the correlations of the disorder do not introduce another macroscopic length scale. If such a scale is present, it might induce a time scale $T_1 < T_0$, which sets another upper limit to the region of validity of the blob concept.

As a further, more specific consequence of our model we note the extreme slowness of the crossover from microscopic to macroscopic diffusional behavior. Even for fairly small disorder and not very long chains, this crossover needs more than five decades of time, and this time interval rapidly increases with increasing disorder or chain length. As a consequence, both the numerical and the theoretical results over several decades of t can be represented as effective power laws. In this respect

we recovered our previous prediction [1]. The exponent, however, does not depend on chain length and disorder, but on the time interval and disorder. Indeed, it is a purely effective quantity, not to be mixed up with asymptotic exponents as resulting from a fixed point under the renormalization group. This observation raises strong doubts whether the search for asymptotic exponents, so common in work on the present or closely related topics, really is appropriate.

Renormalizability of our model leads to a universal nonlinear scaling law (4.1). Strictly speaking, our simulations do not check this full law since we did not systematically explore the region of larger time, where the nontrivial $\tilde{N}$ dependence can be seen. In their more restricted range, the data, however, are fully consistent with the theory.

Universality implies that our results should hold also for other distributions of the disorder. In this context the results of [6] are particularly interesting. The Monte Carlo simulation described in that work uses the same type of a pearl-necklace chain as employed here. The disorder, however, is modeled by randomly occupying cells with impenetrable obstacles (i.e., $V_{\mathbf{n}} = 0$ or ∞). Even though for $d = 3$ this does not introduce truly topological disorder, this model is closer to reptation, since the chain cannot penetrate the obstacles. As judged by comparing Fig. 1 of Ref. [6] with Fig. 6 of the present paper, the results nevertheless are most similar to those presented here. Specifically, the asymptotic diffusional regimes are connected by a large interval of very smooth crossover. The asymptotic long-time diffusion sets in only for $t \gtrsim 10T_0$ and a large part of the crossover region could well be represented by a power law. Furthermore, the blob model law $R^2(t) \sim f(t)/N$ clearly holds until the curves finally bend over to the asymptotic diffusional behavior. This strongly suggests that our results, and in particular our description of the crossover towards asymptotic diffusion, indeed are universal, valid for a large class of models.

We finally should compare our results to those of the reptation model [7,3]. This model introduces another important time scale T_e defined such that the size of the time blobs for $t \approx T_e$ reaches the size of the tube built up by the topological constraints. The time T_0, where the chain has moved a distance of the order of its size, becomes the reptation time, increasing proportional to N^3. For $R^2(t)$ the model predicts the diffusional behavior $R^2(t) \approx D_{\mathrm{rep}}t$ for $t > T_1$, $D_{\mathrm{rep}} \propto 1/N^2$, which should set in long before the chain has moved a distance of order R_G^2. Indeed, from the arguments of [3] we would estimate T_1 to lie in the interval $T_e < T_1 < T_0/N$. This indeed is seen in the work of [17], where the polymer chains move through a regular lattice of obstacles. For the more commonly employed irregular distribution of obstacles, asymptotic diffusion seems to set in much later. The curves of Ref. [8], Fig. 1, for instance, show a behavior of $R^2(t)$ most similar to that found here, though there the reptationlike motion of a chain through a two-dimensional disordered system of obstacles has been simulated. Normal diffusion sets in for $T \gtrsim 10\ T_0$, T_0 scaling like N^3. This suggests that disorder in the distribution of obstacles strongly influences the motion of the chains, a conclusion also reached in a recent Letter [10]. We might hope that the present theory is helpful in understanding that behavior, concentrating on the universal effects of the disorder.

ACKNOWLEDGMENTS

U.E. and L.S. are indebted to the Sonderforschungsbereich 237 of the Deutsche Forschungsgemeinschaft for financial support. U.E. furthermore gratefully acknowledges financial support by the Nederlandse Organisatie voor Wetenschappelijk Onderzoek during the completion of this work. Beyond that, she wants to thank W. van Saarloos for numerous discussions about the implications of this research. The computer simulations have been performed on the IBM ES-9000 at the Forschungszentrum Jülich.

APPENDIX: RENORMALIZATION GROUP FLOW

The general form of the flow equation for the disorder strength $\bar{v}(\lambda), \lambda = \ell_R/\ell$, reads

$$\lambda \frac{d}{d\lambda}\bar{v}(\lambda) = W_v(\bar{v}(\lambda), \bar{w}(\lambda)) \quad . \tag{A1}$$

Assuming that $\bar{w}(\lambda)$ takes its fixed point value $\bar{w}(\lambda) \equiv \bar{w}^*$, we easily can integrate this equation to find the formal result

$$\lambda = \frac{F_v(\bar{v}(\lambda))}{F_v(\bar{v}(1))} \quad , \tag{A2}$$

where

$$\ln F_v(\bar{v}) = \int^{\bar{v}} \frac{dx}{W_v(x, \bar{w}^*)} \quad . \tag{A3}$$

To three-loop order the result for W_v may be found in the appendix of Ref. [12]. [$W_v(\bar{v}, \bar{w}) \equiv \hat{W}_{12}(\bar{w}, \bar{w}, -\bar{v})$ in the notation of that paper, Eq. (A17).] Specializing the analysis given there to $W_v(\bar{v}, \bar{w}^*)$, we introduce the derivatives

$$\omega_{12}^{(0)} = \frac{\partial}{\partial \bar{v}} W_v(\bar{v}, \bar{w}^*)\Big|_{\bar{v}=0} \equiv d - \frac{2}{\nu} \quad , \tag{A4}$$

$$\omega_{12}^{*} = \frac{\partial}{\partial \bar{v}} W_v(\bar{v}, \bar{w}^*)\Big|_{\bar{v}=-\bar{w}^*} \quad , \tag{A5}$$

where the last identity in Eq (A4) has been proven in [18]. $\bar{v} = -\bar{w}^*$ is the nontrivial zero of $W_v(\bar{v}, \bar{w}^*)$. For $d = 3$ we find $\omega_{12}^{(0)} = -0.40 = -\omega_{12}^*$, where by pure accident $\omega_{12}^{(0)} \approx -\omega_{12}^*$. This simplifies the further analysis. We then write

$$W_v(\bar{v}, \bar{w}^*) = -\omega_{12}^* \bar{v} \left(1 + \frac{\bar{v}}{\bar{w}^*}\right) \quad . \tag{A6}$$

This relation reproduces the two-loop result and is a good approximation to the three-loop result. Equations (A3) and (A6) yield

$$F_v(\bar{v}) = \bar{v}^{-1/\omega_{12}^*}(1+\bar{v}/\bar{w}^*)^{1/\omega_{12}^*} \quad . \tag{A7}$$

Introducing $s_v = F_v(\bar{v}(1))$, we then may solve Eq. (A2) to find

$$\bar{v}(\lambda) = \left((s_v\lambda)^{\omega_{12}^*} - \frac{1}{\bar{w}^*}\right)^{-1} \quad . \tag{A8}$$

We now turn to the equation for γ_R/n_R. From [1,2] we take the result

$$\lambda\frac{d}{d\lambda}\ln\frac{\gamma_R(\lambda)}{n_R(\lambda)} = W_\gamma(\bar{v}(\lambda),\bar{w}(\lambda)) = I\bar{v}(\lambda) + \mathcal{O}(\bar{v}^2,\bar{v}\bar{w}), \qquad I = 3.587 \quad . \tag{A9}$$

Specializing to $\bar{w}(\lambda) \equiv \bar{w}^*$, we may use the standard procedure of eliminating $\lambda d/d\lambda$ in favor of d/dv to find, after a simple integration,

$$\frac{\gamma_R(\lambda)}{n_R(\lambda)} = \frac{F_\gamma(\bar{v}(\lambda))}{F_\gamma(\bar{v}(1))}\frac{\gamma_R(1)}{n_R(1)} \quad , \tag{A10}$$

$$\ln F_\gamma(\bar{v}) = \int^{\bar{v}} dx\,\frac{W_\gamma(x,\bar{w}^*)}{W_v(x,\bar{w}^*)} \quad . \tag{A11}$$

With $n_R(\lambda) = (s_v\lambda)^{1/\nu}\tilde{N}$ and $\tilde{\gamma} = s_v^{-1/\nu}F_\gamma^{-1}(\bar{v}(1))\,\gamma_R(1)$, Eq. (A10) is written as

$$\gamma_R(\lambda) = (s_v\lambda)^{1/\nu}F_\gamma(\bar{v}(\lambda))\tilde{\gamma} \quad . \tag{A12}$$

Inserting approximations (A6) and (A9), Eq. (A11) yields

$$F_\gamma(\bar{v}) = (1+\bar{v}/\bar{w}^*)^{-\sigma/\omega_{12}^*} \quad , \tag{A13}$$

$$\sigma = \bar{w}^*I = \frac{\epsilon}{4}I + O(\epsilon^2) \quad . \tag{A14}$$

[1] U. Ebert and L. Schäfer, Europhys. Lett. **21**, 741 (1993); L. Schäfer and U. Ebert, Makromol. Chem. Macromol. Symp. **81**, 17 (1994).
[2] U. Ebert, J. Stat. Phys. **82**, 183 (1996).
[3] M. Doi and S.F. Edwards, *The Theory of Polymer Dynamics* (Clarendon, Oxford, 1986).
[4] U. Ebert and L. Schäfer, Makromol. Chem. Macromol. Symp. **81**, 31 (1994).
[5] A. Baumgärtner and M. Muthukumar, J. Chem. Phys. **87**, 3082 (1987); M. Muthukumar and A. Baumgärtner, Macromolecules **22**, 1937 (1989).
[6] M. Muthukumar and A. Baumgärtner, Macromolecules **22**, 1941 (1989).
[7] P.G. de Gennes, J. Chem. Phys. **55**, 572 (1971).
[8] A. Baumgärtner, Europhys. Lett. **4**, 1221 (1987).
[9] B.H. Zimm and O. Lumpkin, Macromolecules **26**, 226 (1993).
[10] G.W. Slater and S.Y. Wu, Phys. Rev. Lett. **75**, 164 (1995).
[11] R. Schloms and V. Dohm, Nucl. Phys. B **328**, 639 (1989).
[12] L. Schäfer and Ch. Kappeler, J. Chem. Phys. **99**, 6135 (1993).
[13] L. Schäfer, Macromolecules **17**, 1357 (1984).
[14] A. Baumgärtner, Annu. Rev. Phys. Chem. **35**, 419 (1984).
[15] K. Kremer, A. Baumgärtner, and K. Binder, Z. Phys. B **40**, 331 (1981).
[16] B.G. Nickel, Macromolecules **24**, 1358 (1991); L. Schäfer, Phys. Rev. E **50**, 3517 (1994).
[17] E. Evans and S.F. Edwards, J. Chem. Soc. Faraday Trans. 2 **77**, 1891 (1981).
[18] L. Schäfer, U. Lehr, and Ch. Kapeller, J. Phys. (France) I **1**, 211 (1991).